J. Appl. Comput. Mech., xx(x) (2026) 1-11
DOI: 10.22055/jacm.2026.49420.5964

ISSN: 2383-4536
jacm.scu.ac.ir

Shahid Chamran University of Ahvaz

Journal of Applied and Computational Mechanics

Research Paper

Experimental–Analytical Identification of Shear Elastic Modulus and Shear Correction Factor in Composite Wind Turbine Blades

Andres Lopez-Lopez[1], Jesus A. Enriquez-Santiago[2], Marco A. Zuñiga-Reyes[3], Marco A. Zamora-Antuñano[4,5], Perla Y. Sevilla-Camacho[6], José B. Robles-Ocampo[7]

[1] Centro de Investigación, Innovación y Desarrollo Tecnológico (CIIDETEC), Universidad del Valle de México (UVM), Campus Online, Av. Marina Nacional 500, Anáhuac I Secc, Miguel Hidalgo, Ciudad de México, 11320, México, Email: andres.lopez@uvmnet.edu

[2] División de Estudios de Posgrado, Universidad del Istmo, Ciudad Universitaria S/N Barrio Santa Cruz 4a. Sección, Sto. Domingo Tehuantepec, Oaxaca, 70760, México, Email: ing.jesusantonio@hotmail.com

[3] Departamento de Metal Mecánica, Tecnológico Nacional de México/IT de Tuxtla Gutiérrez, Carretera Panamericana Km 1080, Tuxtla Gutiérrez C.P. 29050, México, Email: marco.zr@tuxtla.tecnm.mx

[4] Instituto de Investigación e Innovación en Energías Renovables, Universidad Autónoma de Ciencias y Artes de Chiapas, Libramiento norte poniente 1150, Lajas Maciel, Tuxtla Gutiérrez, Chis, 29039, México

[5] Consejo de Ciencia y Tecnología del Estado de Querétaro (CONCYTEQ), Av. Prolongación Luis Pasteur 36, Centro, Santiago de Querétaro 76000, México

[6] Programa Académico de Ingeniería Mecatrónica, Universidad Politécnica de Chiapas, Suchiapa 29150, México, Email: psevilla@upchiapas.edu.mx

[7] Programa Académico de Ingeniería en Manufactura Avanzada, Universidad Politécnica de Chiapas, Suchiapa 29150, México, Email: jrobles@upchiapas.edu.mx

Received May 22 2026; Revised August 05 2026; Accepted for publication September 08 2026.
✉ Corresponding author: J.B. Robles-Ocampo (jrobles@upchiapas.edu.mx)

Abstract. Accurate estimation of the effective shear stiffness of composite wind turbine blades remains challenging because equivalent beam models require reliable shear properties for hollow anisotropic composite structures. This study proposes a hybrid experimental–analytical methodology that integrates experimental modal analysis, laminate-based sectional modeling, and thin-walled shear flow theory to identify the effective shear elastic modulus and determine the shear correction factor. Unlike conventional approaches based on prescribed material properties or simplified assumptions, the proposed framework directly links experimental dynamic response with equivalent structural parameters. The identified shear elastic modulus shows deviations below 1.1% across vibration modes. The methodology improves the accuracy of equivalent Timoshenko beam models for structural characterization, vibration analysis, and structural health monitoring of composite wind turbine blades.

Keywords: Composite wind turbine blades; Shear elastic modulus identification; Shear correction factor; Hollow aerodynamic sections; Experimental modal analysis; Thin-walled composite structures.

1. Introduction

Composite wind turbine blades (CWTBs) are critical structural components whose dynamic behavior directly influences the reliability, efficiency, and operational safety of wind turbine energy systems. Accurate structural modeling is therefore essential for predicting vibration response, assessing structural integrity, and preventing resonance-related failures during service. However, the mechanical characterization of these structures remains challenging due to their complex aerodynamic geometry, spanwise variation in cross-sections, and the pronounced anisotropy inherent to laminated composite materials.

In engineering practice, wind turbine blades (WTB) are commonly modeled as equivalent beams with spatially varying sectional properties. Among the most widely used formulations, Timoshenko beam theory provides an improved representation by accounting for both bending and transverse shear deformation, particularly relevant in composite structures with relatively low shear stiffness. Nevertheless, the predictive accuracy of such models strongly depends on the reliable estimation of equivalent sectional properties, especially the shear stiffness and the associated shear correction factor.

Determining the equivalent mechanical properties of CWTBs remains inherently challenging because their structural response is governed by fiber orientation, stacking sequence, and interlaminar interactions, which produce pronounced anisotropic behavior and stiffness coupling. Consequently, material properties obtained from coupon tests do not necessarily represent the equivalent structural properties of full-scale blades, particularly for hollow geometries [1]. Previous studies have reported discrepancies between static and dynamic elastic properties, indicating that conventional material characterization may not accurately capture the effective structural response. The influence of laminate architecture on the dynamic behavior of composite structures has

Published online: September 19 2026

therefore been extensively investigated. Instrumented impact tests and frequency-based analyses demonstrated significant differences between the longitudinal elastic modulus and the shear elastic modulus (SEM) [2, 3], while several vibration-based methodologies have been proposed to identify equivalent elastic properties in multilayer materials and beam-like structures [4, 5]. Although these studies confirm the potential of modal analysis for non-destructive characterization, they mainly focus on Young's modulus and do not directly estimate the effective SEM required for equivalent Timoshenko beam models.

Building upon these developments, vibration-based techniques have been combined with numerical modeling to estimate the equivalent mechanical properties of composite structures. Apsan et al. [6] determined the EM of fiber-reinforced composites through natural frequency analysis, while Loh et al. [7] integrated digital image correlation with finite element modeling to identify elastic properties from free vibration tests in cantilever beams. Although these methodologies have demonstrated good accuracy, they generally rely on simplified beam formulations that neglect transverse shear deformation. Consequently, the structural representation adopted in equivalent beam models remains a major source of uncertainty. Euler–Bernoulli beam theory neglects transverse shear deformation and rotary inertia, which may introduce significant errors when applied to CWTB with moderate slenderness ratios [8]. In contrast, sectional modeling approaches based on Classical Laminate Theory (CLT) and thin-walled beam formulations have significantly improved the estimation of bending stiffness, mass distribution, and equivalent sectional properties [9]. Nevertheless, many existing formulations still rely on Euler–Bernoulli assumptions, motivating the use of Timoshenko beam theory together with reliable estimation of the shear correction factor. Accordingly, considerable efforts have been devoted to developing analytical [10], numerical, and energy-based formulations [11] for determining shear correction factors in thin-walled sections.

Although these formulations have significantly advanced the estimation of shear correction factors, their application to aerodynamic composite sections remains limited. Existing studies have mainly focused on solid or isotropic airfoil configurations. Freund et al. [12] demonstrated that the shear correction factor is strongly influenced by cross-sectional geometry in thin-walled profiles, although their analysis was limited to open and isotropic sections. Likewise, Dong et al. [13], Kirad et al. [14], and Zefouni et al. [15] investigated the determination of shear correction factors and shear stress distributions in solid or symmetric airfoil sections using analytical and numerical approaches. However, these studies do not consider hollow, multi-cell sections composed of anisotropic composite laminates, which are characteristic of modern CWTB.

A key limitation in most studies is that sectional properties used in beam models are determined a priori from numerical simulations or material data. At the same time, experimental modal analysis is employed only as a validation tool. Consequently, the direct identification of effective shear stiffness from experimental dynamic response remains limited in the literature, particularly for hollow composite sections in WTB.

To address these limitations, this study proposes an integrated experimental–analytical framework for CWTBs. Unlike existing approaches based on prescribed shear correction factors, conventional cross-sections, or detailed finite-element models, the proposed method determines direction-dependent shear correction factors from the geometry, laminate distribution, and shear-flow energy, while identifying the dynamic SEM from experimental natural frequencies. Its novelty and analytical distinction lie in independently determining and subsequently integrating these parameters, together with spanwise-varying sectional properties, into an equivalent Timoshenko beam model for hollow anisotropic blades. From an engineering perspective, the framework provides a computationally efficient means of obtaining blade-specific structural parameters for vibration prediction, structural design, finite-element model updating, and structural health monitoring.

2. Material and Methods

Figure 1 illustrates the methodological framework used to determine the effective SEM of the WTB by combining experimental modal analysis with sectional structural analysis. The procedure begins with an experimental modal test in which the WTB is mounted as a cantilever structure and excited using an impact hammer. The dynamic response is measured to identify the natural frequencies and corresponding vibration modes of the WTB. These experimentally obtained frequencies are then used to determine an experimental modal parameter that characterizes the structure's dynamic behavior.

In parallel, a sectional structural analysis of the WTB is performed. The airfoil geometry is discretized into multiple segments to evaluate the sectional mechanical properties. In contrast, the effective properties of the composite laminate are determined by the stacking sequence and material properties of the layers. A shear-flow analysis of the closed thin-walled section is then performed to determine the equivalent structural properties of the WTB. As part of this process, the shear correction factor for hollow composite airfoil sections is determined, enabling the evaluation of the effective shear stiffness required in the equivalent beam formulation. This procedure enables the estimation of the shear correction factor for complex hollow WTB sections, which is rarely reported in experimental–analytical studies of CWTB.

Finally, the experimentally derived modal parameter is related to the equivalent beam formulation to estimate the effective SEM of the WTB. The obtained SEM is subsequently compared with the sectional properties to verify consistency between the dynamic response and the WTB's structural parameters.

2.1. Structural dynamic model

The dynamic behavior of the structural system is initially modeled using the classical Euler–Bernoulli beam theory. Eq. (1) gives the differential equation governing transverse vibration for a uniform beam [16]:

$$EI\frac{\partial^4 w(x,t)}{\partial x^4} + \rho A\frac{\partial^2 w(x,t)}{\partial t^2} = 0 \tag{1}$$

where E is the EM, I is the area inertia moment, ρ is the material density, A is the cross-sectional area, and $w(x,t)$ denotes the transverse displacement.

The modal solution of Eq. (1) yields the natural frequencies, as given in Eq. (2):

$$f_n = \frac{\beta_n^2}{2\pi L^2}\sqrt{\frac{EI}{\rho A}} \tag{2}$$

where β_n depends on the system's boundary conditions. From Eq. (2), a dimensionless modal parameter can be defined as [4]:

$$(\beta L)_n^2 = \frac{2\pi f_n L^2}{\sqrt{\frac{\mathrm{EI}}{\rho A}}} \tag{3}$$

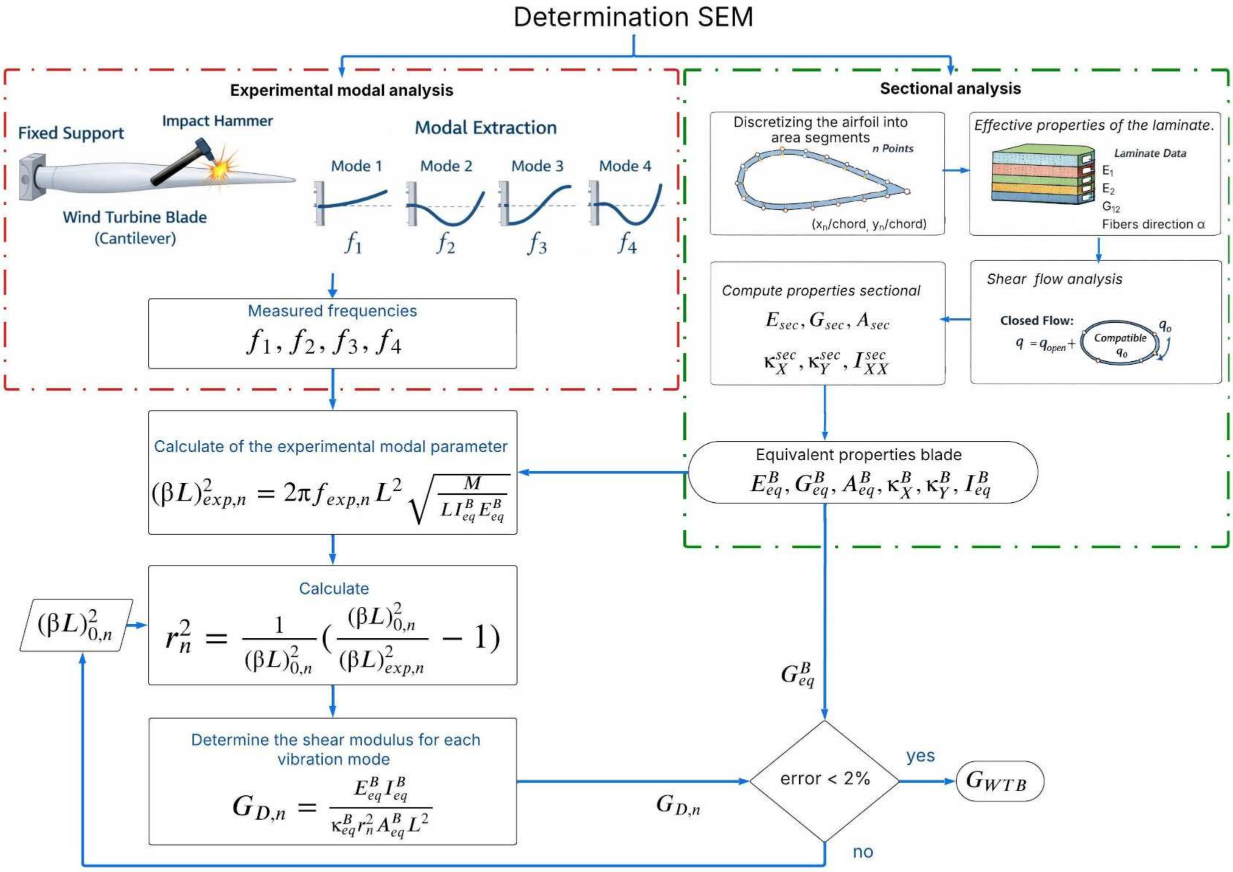

Fig. 1. Methodological framework for estimating the SEM of the WTB using experimental modal analysis and sectional structural analysis.

This modal parameter, $(\beta L)^2$, represents a normalized natural frequency and links the structure's dynamic response to its stiffness-to-mass ratio.

The Euler–Bernoulli beam model neglects transverse shear deformation, which may become significant in CWTB with moderate slenderness ratios. To account for this effect, Timoshenko beam theory introduces an effective shear rigidity κGA, where G is the SEM and κ is the shear correction factor [17].

The relative importance of shear deformation with respect to bending is quantified by the dimensionless parameter r^2 [18]:

$$r^2 = \frac{EI}{\kappa GAL^2} \tag{4}$$

This parameter represents the ratio between bending and shear stiffness, thereby indicating the contribution of transverse shear deformation to the dynamic response of the structure.

2.2. Experimental modal parameter extraction

The schematic in Fig. 2 illustrates the experimental setup for the dynamic characterization of CWTB through modal vibration testing. The WTB was rigidly clamped at the root in a horizontal cantilever configuration, with a 0.10 m clamping length between polystyrene plates (0.20×0.10×0.05 m) using 4 M8 bolts at 30 N·m, yielding a free length of 1.61 m. Since no displacement or rotation was detected at the root, the boundary condition was treated as fixed. A calibrated impact hammer (5000 N, 250 g, type 9724A5000N, 5 mV/N sensitivity) is used to excite the structure at a position 0.10 m from the fixed support, inducing multiple vibration modes. The impact was applied in a flapwise direction. The response is measured using a piezoelectric accelerometer (Kistler 8440A5, 1067 mV/g) mounted at 1.07 m from the fixed support, on the deck surface, and aligned with the excitation direction. Both signals are acquired using a 24-bit data acquisition (DAQ) system with a maximum sampling rate of 200 kS/s per channel, controlled via KiStudio Lab Package Type 2910A. The data were acquired at 2048 Hz for 8 s. Five valid impacts were averaged, applying a force window to the hammer and an exponential window to the acceleration. The FRFs were obtained by identifying resonance peaks in the 0–60 Hz range. Double impacts and coherence values < 95% were discarded.

From the measured frequencies f_n, the experimental modal parameter is determined using Eq. (5):

$$(\beta L)^2_{exp,n} = 2\pi f_{exp,n} L^2 \sqrt{\frac{M}{L I_{eq}^B E_{eq}^B}} \tag{5}$$

2.3. Inverse identification of shear elastic modulus

To estimate the SEM of the structural system, an inverse identification procedure based on vibration measurements was employed. The approach correlates the experimental modal parameter with the theoretical Euler–Bernoulli value via an algebraic correction that accounts for shear deformation, as described by Timoshenko beam theory.

Physically, this formulation exploits the fact that deviations between the experimental modal response and the Euler–Bernoulli prediction arise from shear flexibility, which reduces the natural frequencies. This effect is quantified by the dimensionless parameter r^2, which represents the relative contribution of shear deformation to bending.

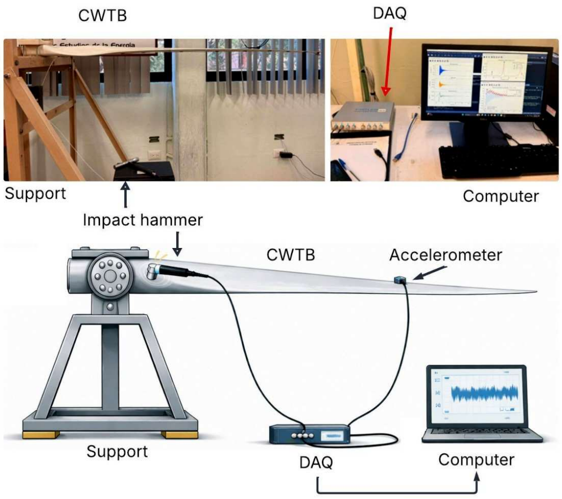

Fig. 2. Modal testing setup of a cantilevered CWTB using impact excitation and accelerometer response measurement.

The relationship used is given by Eq. 6, where $(\beta L)_{0,n}$ represents the theoretical Euler–Bernoulli modal parameter:

$$(\beta L)_n^2 = \frac{(\beta L)_{0,n}^2}{1 + r^2(\beta L)_{0,n}^2} \tag{6}$$

Substituting the experimental value of the modal parameter into the above equation yields:

$$r_n^2 = \frac{1}{(\beta L)_{0,n}^2}\left(\frac{(\beta L)_{0,n}^2}{(\beta L)_{exp,n}^2} - 1\right) \tag{7}$$

Once r_n^2 is determined, the dynamic SEM G_D is computed using Eq. (8), representing the effective shear stiffness that reproduces the measured dynamic behavior of each vibration mode:

$$G_{D,n} = \frac{I_{eq}^B E_{eq}^B}{\kappa_{eq}^B r_n^2 A_{eq}^B L^2} \tag{8}$$

The identified elastic modulus should be interpreted as an equivalent dynamic SEM of the WTB, reflecting the global structural response rather than the intrinsic property of an individual laminate layer.

2.4. Torsional stiffness

The hollow WTB, with no internal reinforcements, has a closed cross-section as illustrated in Fig. 3(a). In this configuration, the SEM flow is distributed over the entire enclosed area. Here, ds represents the differential length along a path s that describes the airfoil profile, and ϵ denotes the total thickness of the laminated composite layers that make up the WTB shell at this cross-section. The elastic center is denoted by X and Y.

For a single-cell closed section, the torsional stiffness is given by Bredt–Batho theory, and the shear stiffness GJ can be calculated as shown in Eq. (9), where G is the local SEM, A^* is the area enclosed by the midline of the airfoil and J is the torsional constant:

$$GJ \;=\; 4\;A^{*2} / \oint \frac{1}{\epsilon G} ds \tag{9}$$

2.4.1. *Shear correction factors*

The shear flow $q(s)$ is given by Eq. (10), where $q_{\text{op}}(s)$ is the shear flow of an open cross-section:

$$q(s) \;=\; q_{op}(s) \;+\; q_0 \tag{10}$$

The redundant constant q_0 satisfies the compatibility condition as expressed in Eq. (11):

$$q_0 = -\frac{\left(\oint \frac{q_{op}}{G\epsilon} ds\right)}{\oint \frac{1}{G\epsilon} ds} \tag{11}$$

In this way, the strain energy U due to shear can be expressed in terms of the shear flow $q(s)$ as given in Eq. (12):

$$U \;= \oint \frac{q(s)^2}{2G\epsilon} ds \tag{12}$$

The effective shear stiffness, K_s, is obtained by equating the actual shear strain energy of the cross-section to that of an equivalent Timoshenko beam. In Eq. (13), V is the resultant transverse shear force and U is the corresponding shear strain energy calculated from Eq. (12). For a thin-walled closed section, the material area is evaluated as $A = \oint \epsilon\,(s)\,ds$:

$$K_s = \frac{V^2}{2U} \tag{13}$$

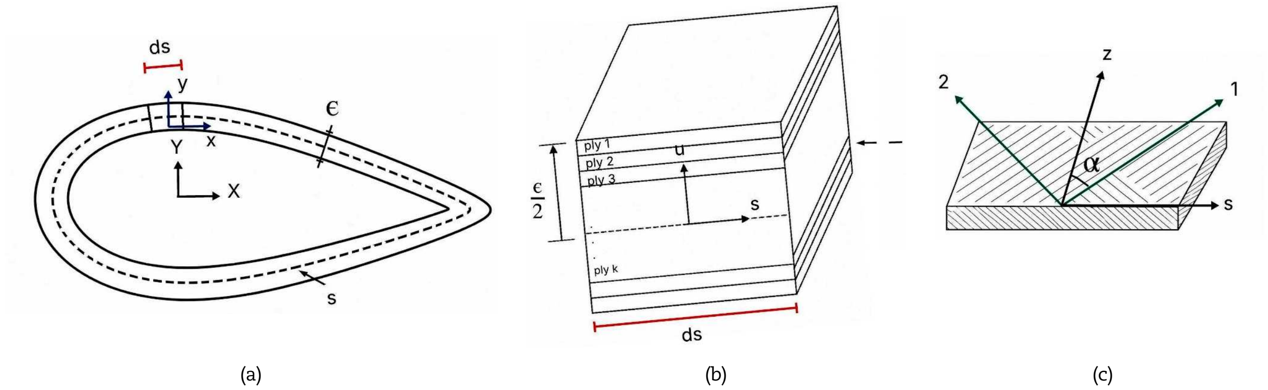

Fig. 3. Characteristics of the composite aerodynamic profile and laminate, (a) Distribution of SEM flow over a typical airfoil, (b) Distribution of laminated layers in a ϵds section of the airfoil perimeter, (c) Fiber orientation of the laminate plies in the 1-2 directions within a local *s*-*z* coordinate plane, where *s* is tangent to the airfoil profile.

The shear correction factor κ is finally defined in Eq. (14), where $\widetilde{GA}$ is the average shear rigidity of the section is, assuming a uniform shear distribution over the entire cross-section:

$$\kappa = \frac{K_s}{\widetilde{GA}} \tag{14}$$

2.5. Cross-section properties

To determine the cross-sectional properties of the WTB, considering its anisotropy and the effects of shear redistribution in closed sections, the methodology proposed in [19] is adopted. This approach incorporates CLT into the framework of thin-walled beam theory. The methodology is modified for application to hollow WTB as described in [9] and is further extended to compute the shear correction factor.

The procedure begins by discretizing the laminates into area segments, each containing angled plies. The engineering constants of the plies are obtained using CLT. A weighting method is then applied to determine the equivalent properties of each segment and the location of the elastic center of the cross-section. First, the area inertia moments of each segment are computed with respect to its local axes and centroid. These values are subsequently transformed to elastic axes and center using axis transformation formulas and the parallel axis theorem. The contribution of each segment to the overall cross-sectional properties is then determined based on these transformed moments and the equivalent segment properties.

The torsional stiffness is obtained using Bredt-Batho shear flow theory (BSFT) for hollow sections. While the other cross-sectional properties are computed by summing the contributions of all area segments, a SEM correction factor for Timoshenko beams is subsequently proposed. Several steps of the procedure for calculating sectional properties are outlined below; the complete methodology is detailed in [20].

Calculate the effective properties of the laminate. The effective longitudinal EM of a ply oriented at an angle α is obtained using Eqs. (15) and (16), and the orientation of the laminate in the local coordinate plane is illustrated in Fig. 3(c):

$$E_z^{ply,} = \frac{1}{\dfrac{cos^4(\alpha)}{E_1} + \left(\dfrac{1}{G_{12}} - \dfrac{2\nu_{12}}{E_1}\right) sin^2(\alpha)cos^2(\alpha) + \dfrac{sin^4(\alpha)}{E_2}} \tag{15}$$

$$G_{xy}^{ply} = \frac{1}{\left(\dfrac{4}{E_2} + \dfrac{4+8\nu_{12}}{E_1} - \dfrac{2}{G_{12}}\right) sin^2(\alpha)cos^2(\alpha) + \dfrac{sin^4(\alpha)+cos^4(\alpha)}{G_{12}}} \tag{16}$$

Calculate equivalent properties of the segment. For each wall segment, the equivalent properties are determined through a thickness-weighted average (see Fig. 3(b)). The properties of each segment are calculated using Eqs. (17) to (19) within a local x-y coordinate system:

$$E_{seg} = \frac{\sum_{k=1}^{m} E_{z,k}^{ply} \epsilon_k^{ply}}{\sum_{k=1}^{m} \epsilon_k^{ply}} \tag{17}$$

$$G_{seg} = \frac{\sum_{k=1}^{m} G_{xy,k}^{ply} \epsilon_k^{ply}}{\sum_{k=1}^{m} \epsilon_k^{ply}} \tag{18}$$

$$\rho_{seg} = \frac{\sum_{k=1}^{m} \rho_k^{ply} \epsilon_k^{ply}}{\sum_{k=1}^{m} \epsilon_k^{ply}} \tag{19}$$

Calculate elastic center: the elastic center coordinates are determined by Eqs. (20) and (21):

$$X_E = \frac{\sum_{I=1}^{N} \mathrm{E}_{seg,I} \mathrm{A}_{seg,I}\ \bar{x}_{seg,I}}{\sum_{I=1}^{N} \mathrm{E}_{seg,I} \mathrm{A}_{seg,I}} \tag{20}$$

$$Y_E = \frac{\sum_{I=1}^{N} \mathrm{E}_{seg,I} \mathrm{A}_{seg,I}\ \bar{y}_{seg,I}}{\sum_{I=1}^{N} \mathrm{E}_{seg,I} \mathrm{A}_{seg,I}} \tag{21}$$

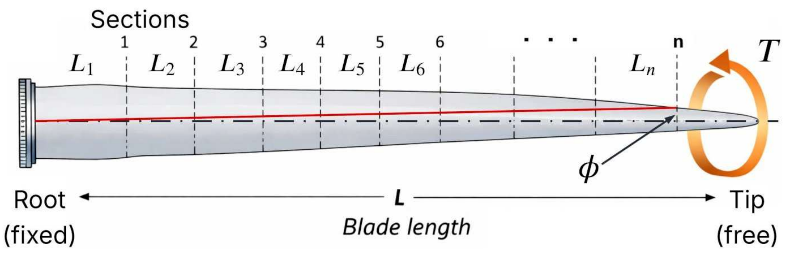

Fig. 4. WTB with variable sectional properties, subjected to a constant torque T.

Translation of the inertia moment to the elastic center: second moments of area of section are computed about the elastic center and are determined by the Eqs. (22) and (23):

$$I_{XX}^{sec} = I_{\mathrm{XX}}^{seg} + \mathrm{A}_{seg}(\bar{y}_c^{seg} - Y_E)^2 \tag{22}$$

$$I_{YY}^{sec} = I_{\mathrm{YY}}^{seg} + \mathrm{A}_{seg}(\bar{x}_c^{seg} - X_E)^2 \tag{23}$$

where I_{XX}^{seg}, I_{YY}^{seg} are the inertia moments about the axes parallel to X and Y, A_{seg} is the area, and $\bar{x}_c^{seg}$, $\bar{y}_c^{seg}$are the x and y centroids of the segments.

Sum contributions of all area segments: Using Eqs. (24) to (27). The properties of each section are calculated from the contribution of the individual sections to obtain the overall sectional properties:

$$\mathrm{E}_{Sec} = \frac{\sum_{I=1}^{N} \mathrm{E}_{seg,I}\mathrm{A}_{seg,I}}{\sum_{I=1}^{N} \mathrm{A}_{seg,I}} \tag{24}$$

$$\mathrm{G}_{Sec} = \frac{\sum_{I=1}^{N} \mathrm{G}_{seg,I}\mathrm{A}_{seg,I}}{\sum_{I=1}^{N} \mathrm{A}_{seg,I}} \tag{25}$$

$$EI_X = \sum_{I=1}^{N} \mathrm{E}_{seg,I} I_{XX}^{sec,I} \tag{26}$$

$$EI_Y = \sum_{I=1}^{N} \mathrm{E}_{seg,I} I_{YY}^{sec,I} \tag{27}$$

Calculate the torsional stiffness using BSFT. Torsional stiffness is determined with the BSFT method for a hollow cross-section of the WTB, such as the one shown in Fig. 3(a). Once the width of each segment $\mathrm{d}s$, its equivalent thickness ϵ_{seg}, and its equivalent SEM G_{seg} are obtained, the torsional stiffness is then calculated using Eq. (9).

Determine the shear stiffness correction factor. The shear correction factor is determined using the SEM flow theory described in section 2.4.1, as given by Eq. (14).

2.6. Equivalent torsional stiffness of a variable-section WTB

A WTB has a variable cross-section along its length, as shown in Fig. 4. If the WTB is subdivided into n sections, each section consists of an airfoil with a different chord and twist angle, resulting in variable sectional properties. To calculate the overall properties of the WTB, an equivalent WTB model is proposed, based on the equivalent beam methodology described in [21].

For a beam with variable cross-sections subjected to a constant torque T , the total angle of twist ϕ is the sum of the twists of each segment. As shown in Eq. (28):

$$\phi = \mathrm{T}\sum_{i=1}^{n} \frac{L_i}{GJ_i} \tag{28}$$

where L_i is the length of the i-th segment, G is the SEM, and J_i is the torsion constant of the section. For an equivalent uniform beam of total length $L\ = \sum L_i$ and torsional stiffness GJ_{eq}, the angle of twist is expressed in Eq. (29):

$$\phi_{eq} = \frac{TL}{GJ_{eq}} \tag{29}$$

Equating both twists ($\phi_{eq} = \phi$) ensures that the equivalent beam preserves the global torsional response of the variable-section WTB. The resulting equivalent torsional stiffness is given by Eq. (30), considering the variation of the SEM G along the blade:

$$GJ_{eq}^{B} = \frac{L}{\sum_{i=1}^{n} \frac{L_i}{G_{Sec,i}\ \ J_{Sec,i}}} \tag{30}$$

The equivalent shear elastic modulus G_{eq} is obtained as a length-weighted average of the sectional values $G_{\mathrm{Sec},i}$, preserving the global torsional response of the variable-section WTB, as expressed in Eq. (31):

$$G_{eq}^{B} = \frac{\sum_{i=1}^{n} G_{Sec,i} L_i}{L} \tag{31}$$

The equivalent properties of a beam with variable cross-sections E_{eq}^{B}, I_{eq}^{B}, and A_{eq}^{B} are determined by the equations described in [21].

Table 1. Geometric characteristics of the WTB: chord, twist angle, and sectional profile.

L [m]	Chord [m]	Twist [°]	Airfoil
0.000	0.12100	0.00	Rectangular
0.115	0.12100	0.00	Rectangular
0.235	0.15058	14.20	
0.340	0.17222	21.00	
0.425	0.16618	17.20	
0.510	0.15500	13.40	
0.595	0.14563	11.15	
0.680	0.13740	8.90	
0.750	0.13035	7.79	
0.850	0.11842	6.20	
0.935	0.11022	5.40	WORTMANN
1.020	0.10154	4.60	FX63-137
1.105	0.09329	4.05	
1.190	0.08525	3.50	
1.275	0.07694	2.95	
1.360	0.06896	2.40	
1.445	0.06047	1.95	
1.530	0.05233	1.50	
1.615	0.04415	1.20	
1.700	0.03674	1.10	

Table 2. Distribution of laminate properties, thickness, and directional angles for Glass Fiber Reinforced Polymer (GFRP) laminates used in WTB manufacturing.

Properties	Glass Fiber Reinforced Polymer (GFRP) laminates													
Laminate	1	2	3	4	5	6	7	8	9	10	11	12	13	14
Direction (°)	45/-45	0	0	45/-45	0	45/-45	0	45/-45	0	0	45/-45	0	45/-45	0
Thickness (mm)	0.6	0.3	0.3	0.6	0.3	0.6	0.3	0.6	0.3	0.3	0.6	0.3	0.6	0.3
Start/End (m)	0/750	0/750	0/1666	0/1666	0/1666	0/1666	0/1666	0/750	0/750	0/1666	0/1666	0/1666	0/1666	0/1666
E_1/E_2 (GPa)	11.5/11.5	31.3/9	31.3/9	11.5/11.5	31.3/9	11.5/11.5	31.3/9	11.5/11.5	31.3/9	31.3/9	11.5/11.5	31.3/9	11.5/11.5	31.3/9
G_{12} (GPa)	9.5	8	8	9.5	8	9.5	8	9.5	8	8	9.5	8	9.5	8
υ_{12}	0.49	0.25	0.25	0.49	0.25	0.49	0.25	0.49	0.25	0.25	0.49	0.25	0.49	0.25
ρ (kg/m³)	1780	1780	1780	1780	1780	1780	1780	1780	1780	1780	1780	1780	1780	1780

3. Results and Discussion

The analyzed WTB belongs to a 1.5 kW wind turbine. It has a length of 1.7 m and a mass of 3.3 kg. Its geometric characteristics are described in Table 1, which details the distribution of chord lengths and design angles along its length, as well as the airfoil profile used in each section. Furthermore, the distribution of Glass Fiber Reinforced Polymer (GFRP) laminates used in the WTB manufacturing is presented in Table 2. Two types of laminates were employed: unidirectional laminate oriented at 0° with respect to the WTB's longitudinal axis, and biaxial laminate oriented at (45°, -45°).

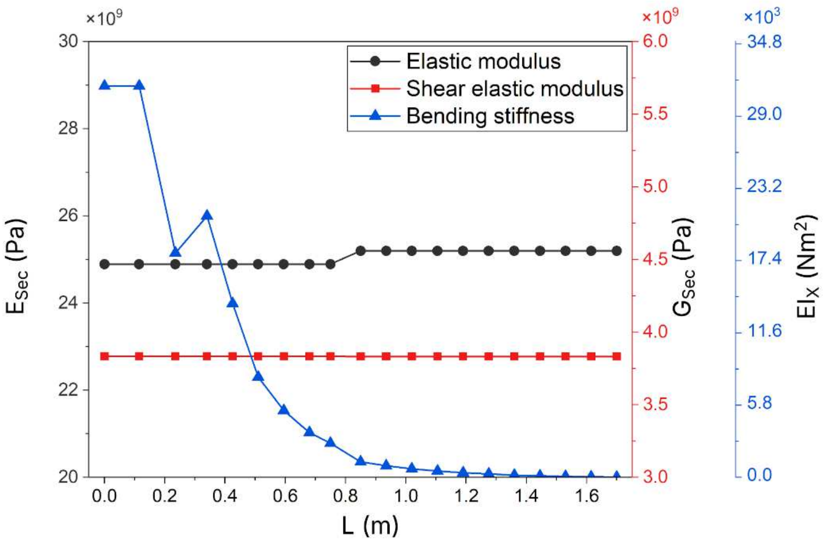

Fig. 5. Distribution of sectional mechanical properties along the WTB.

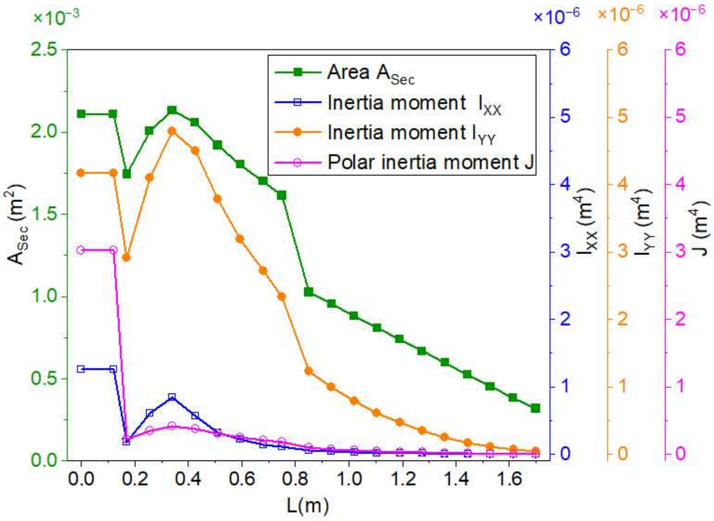

Fig. 6. Variation of sectional properties along the WTB length: cross-sectional area (A), inertia moments I_{XX} and I_{YY}, and polar moment J.

3.1. Sectional analysis CWTB

Figure 5 shows the distribution of sectional mechanical properties along the WTB, from the root (L = 0) to the tip (L = 1.7 m), obtained using laminate theory and cross-sectional modeling. The horizontal axis represents the longitudinal position L (m). Three properties are presented: the sectional elastic modulus E_{Sec}, the sectional SEM G_{Sec}, and the bending stiffness EI_X.

Both E_{Sec} and G_{Sec} remain nearly constant along the WTB, with values ranging from 2.489×10^{10} to 2.519×10^{10} Pa and approximately 3.8×10^{9} Pa, respectively, indicating a relatively homogeneous laminate configuration. The 1.22% increase in EM beyond 0.750 m is attributed to a reduction in the proportion of bidirectional plies, which exhibit lower longitudinal stiffness than unidirectional plies from 42% in the root sections to 33% toward the tip. The SEM shows minimal sensitivity to laminate configuration, with values remaining approximately constant at 3.8×10^{9} Pa, exhibiting a variation of only 0.04%.

In contrast, the bending stiffness EI_X decreases significantly from the root, with values close to 3.0×10^{4} N·m², to values approaching zero at the tip. This reduction is primarily associated with the progressive decrease in chord length, structural thickness, and second moment of area, while the EM remains effectively constant.

Figure 6 shows the variation of sectional properties along the WTB length. The cross-sectional area is largest at the root (≈ 2.1×10^{-3}m²) and gradually decreases toward the tip, consistent with a design that concentrates structural strength where loads are highest. Similarly, the second moments of area I_{YY} and I_{XX} decrease along the WTB, with I_{YY} being dominant, indicating higher stiffness in the edgewise direction.

The polar inertia moment J exhibits a more pronounced drop, particularly near $L \approx 0.2$ m, due to a geometric transition in the WTB design. Overall, the results reflect a typical WTB distribution, with high stiffness at the root and a gradual reduction toward the tip to optimize mass and aerodynamic performance. However, abrupt variations may influence the structural and dynamic response.

3.2. Shear correction factor

The numerical implementation was validated against published results for box, circular-tube, and WORTMANN FX sections. Relative differences ranged from 0.6% to 3.11% (Table 3), confirming that the formulation reproduces established results for both conventional and aerodynamic geometries. The box formulation in [11] was previously validated with ANSYS (maximum error of 0.6%), so this agreement provides an indirect finite-element reference. However, this does not equate to a 3D validation of the complete blade. The presented approach constitutes an efficient experimental-analytical alternative; a direct comparison with a detailed finite-element model is proposed as future work. After validation, the formulation was applied to the WORTMANN FX profile (for which no reference factors were found). The difference between κ_y and κ_x reflects the directional shear response of the slender, hollow aerodynamic geometry.

Table 4 summarizes the spanwise variation of the section-specific shear correction factors, calculated using the methodology described in Section 2.4.1. Here, $\kappa_Y^{sec}$and κ_X^{sec}correspond to shear deformation along the Y- and X-directions, respectively. A pronounced directional dependence is observed along the blade. From root to tip, κ_Y^{sec}decreases, whereas κ_X^{sec}increases and gradually stabilizes. This behavior is associated with the transition from the rectangular root section to the WORTMANN FX63-137 profile and with the progressive reduction in chord along the blade span.

3.3. Experimental analysis CWTB

Figure 7 shows the WTB response after the impact of hammer excitation. Figure 7(a) indicates that the acceleration exhibits a damped free vibration with decreasing amplitude, ranging from a maximum of 22.43 m/s² to a minimum of 5.75 m/s². The decay reflects energy dissipation due to structural damping, with a damping ratio of ζ = 0.0103. The regularity of the peaks indicates well-defined modes without nonlinear behavior, validating the linear regime for modal analysis. In Fig. 7(b), the frequency spectrum shows peaks at 1.3 Hz, 7.6 Hz (dominant mode), 23 Hz, and 45.5 Hz, which correspond to a flexible structure typical of small-scale WTBs.

Table 3. Validation of shear correction factors for different cross-sections.

Cross section	Literature κ_y/κ_x	Present κ_y/κ_x	Error (%)	Reference
Thin-walled box	0.2232/0.6105	0.2251/0.6142	0.85/0.6	[11]
Circular tube	0.5000/0.5000	0.5054/0.5054	1.1/1.1	[12]
WORTMANN FX	0.9200/0.8900	0.9283/0.9177	0.9/3.11	[15]
Thin walled WORTMANN FX	NA	0.0958/0.7458	NA	Present

Table 4. Distribution of the shear correction factor along the CWTB sections.

L [m]	Chord [m]	κ_Y^{sec}	κ_X^{sec}	Section
0.120	0.121 x 0.055 x 0.006 (b x h x ϵ)	0.2021	0.6357	Rectangular
0.340	0.1752	0.1282	0.7111	WORTMANN FX63-137
0.680	0.1404	0.0462	0.7934	WORTMANN FX63-137
0.935	0.1123	0.0344	0.8053	WORTMANN FX63-137
1.020	0.1036	0.0326	0.8073	WORTMANN FX63-137
1.360	0.0710	0.0290	0.8110	WORTMANN FX63-137
1.700	0.0388	0.0279	0.8121	WORTMANN FX63-137

Table 5. Estimation of the dynamic SEM G_D of the WTB based on modal analysis of the first four vibration modes.

Mode	$f_{exp,n}$	Present $(\beta L)_n$	$(\beta L)_{exp,n}$	Uniform beam [22] $(\beta L)_n$	$G_{D,n}$(GPa)	G_{eq}^B (GPa)	Error (%)
1	1.30	1.657	1.6563	1.8751	3.7919	3.8328	1.0660
2	7.60	3.722	3.7161	4.6941	3.8322	3.8328	0.0160
3	23.0	6.660	6.6231	7.8548	3.8556	3.8328	0.5950
4	45.5	9.370	9.2680	10.995	3.7995	3.8328	0.8680

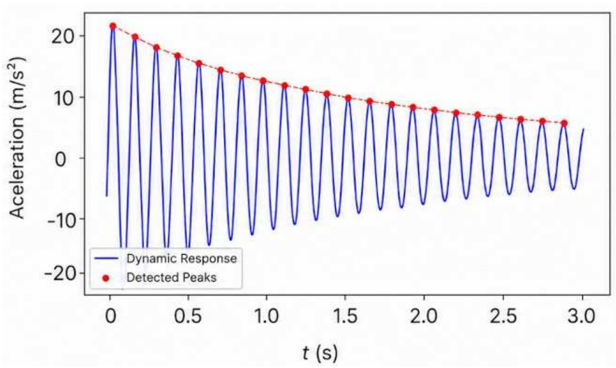

(a)

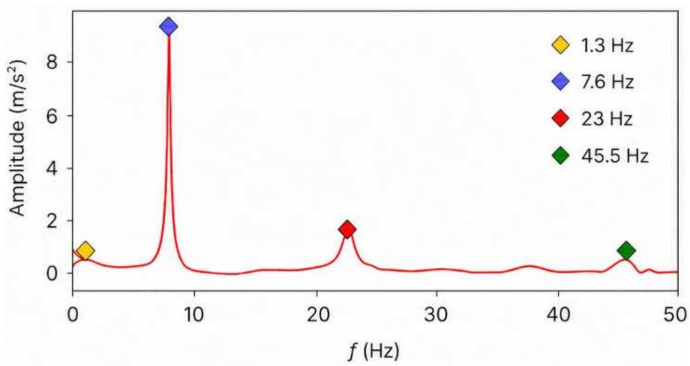

(b)

Fig. 7. Modal response of the CWTB: (a) Damped free vibration in the time domain, (b) Frequency spectrum with identified natural frequencies at 1.3, 7.6, 23, and 45.5 Hz.

3.4. Experimental shear elastic modulus

The dynamic SEM G_D of the WTB was evaluated using the following parameters: $L = 1.7\,\mathrm{m}$, $E_{eq}^B = 25$ GPa, $\rho_{eq}^B = 1780\,\mathrm{kg/m^3}$, mass $M = 3.3\,\mathrm{kg}$, equivalent area $A_{eq}^B = 0.001224\,\mathrm{m^2}$, $I_{eq}^B = 8.23 \times 10^{-9}\,\mathrm{m^4}$. The determination of E_{eq}^B, A_{eq}^B, and $I_{eq;XX}^B$ is described in detail in [9]. The equivalent shear correction factor κ_{eq}^B (Eq. 32) is obtained by condensing the sectional shear correction factors into a single value using a length-weighted average. For the analyzed sections, $\kappa_{eq,Y}^B = 0.06$ (in direction Y) and $\kappa_{eq,X}^B = 0.78$ (in direction X) were obtained:

$$\kappa_{eq}^B = \frac{\sum_i^n \varkappa_i L_i}{\sum_i^n L_i} \tag{32}$$

Table 5 presents the dynamic SEM G_D of the WTB estimated from the first four vibration modes, with experimental natural frequencies of 1.3, 7.6, 23, and 45.5 Hz. The experimental values of $(\beta L)_n^2$ show strong agreement with the corresponding fitted values, confirming the consistency of the inverse identification procedure.

Compared to the uniform beam solution, the theoretical values of $(\beta L)_n^2$ are lower, with differences ranging from 11–20%. This discrepancy is attributed to geometric and stiffness nonuniformity along the WTB, leading to deviations from the constant-section assumption.

The dynamic SEM G_D lies within the range of 3.79–3.86 GPa, with an average value close to $G_{eq}^B = 3.8328\,\mathrm{GPa}$. The relative error remains below 1.1% for all modes, reaching a minimum of 0.016% in the second mode.

These results demonstrate that modal analysis enables highly accurate and robust G_D estimation, with greater reliability from the second mode onward. The low dispersion across modes confirms the validity of the equivalent model and the consistency of the estimated mechanical properties.

4. Conclusion

An experimental–analytical methodology was presented for identifying the effective SEM in CWTB. The following conclusions were drawn:

- The integration of experimental modal analysis with detailed sectional structural modeling enables the accurate and consistent estimation of the dynamic SEM, with deviations below 1.1% across vibration modes, validating the reliability of the proposed procedure.
- The identified SEM exhibits low dispersion (3.79–3.86 GPa), demonstrating the robustness of the methodology, with improved accuracy from the second vibration mode onward.
- The observed differences (11–20%) relative to the uniform beam model highlight the influence of geometric and stiffness

variations along the WTB, confirming the need for models with variable sectional properties.
- The sectional analysis, based on CLT and thin-walled section modeling, accurately captures the distribution of mechanical properties, particularly the progressive reduction in bending stiffness and inertia moments toward the tip, consistent with WTB structural design.
- The proposed formulation for the shear correction factor shows good agreement with reported values for rectangular hollow sections and extends its applicability to anisotropic CWTB geometries. Furthermore, it is demonstrated that this factor varies along the WTB length as a function of sectional geometry, making it a key parameter for accurately representing shear effects in equivalent beam models.

Author Contributions

A. López-López planned the overall scheme, initiated the project, and suggested the experiments to be conducted. J.A. Enríquez-Santiago and J.B. Robles-Ocampo carried out the experiments and analyzed the results. P.Y. Sevilla-Camacho supervised and managed the project. M.A. Zúñiga-Reyes and M.A. Zamora-Antuñano developed the mathematical modeling and examined the theoretical validation. All authors actively participated in writing the manuscript, discussed the results, reviewed the text, and approved its final version.

Acknowledgments

The authors would like to acknowledge the Secretaría de Ciencia, Humanidades, Tecnología e Innovación (SECIHTI), and the Sistema Nacional de Investigadores e Investigadoras (SNII) for their support.

Conflict of Interest

The authors declare no potential conflicts of interest with respect to the research, authorship, and publication of this article.

Funding

The authors received no financial support for the research, authorship, and publication of this article.

Data Availability Statements

The datasets generated and analyzed during the current study are available from the corresponding author upon request.

Nomenclature

$A; A^*$	Cross-sectional area; area enclosed by the airfoil midline [m²]
$A^B_{eq}; A_{seg}$	Equivalent WTB cross-sectional area; segment area [m²]
$E^{ply}_z; E_{sec}; E_{seg}$	Elastic modulus (laminate ply; sectional; segment) [Pa]
$E; E^B_{eq}$	Elastic modulus; equivalent blade elastic modulus [Pa]
$E_1; E_2$	Fiber elastic modulus (directions 1, 2) [Pa]
$EI_X; EI_Y$	Bending stiffness [N.m²]
$f_n; f_{exp}$	Frequency (n = 1, 2, 3, 4); experimental frequency [Hz]
$G; G^B_{eq}$	Shear elastic modulus; equivalent blade shear elastic modulus [Pa]
$G^{ply}_{xy}; G_{Seg}; G_{Sec}$	Shear elastic modulus (laminate ply; sectional; segment) [Pa]
G_D	Dynamic shear elastic modulus [Pa]
G_{12}	Fiber shear elastic modulus [Pa]
$I; I^B_{eq}$	Area inertia moment; equivalent blade area inertia moment [m⁴]
$I^{seg}_{XX}; I^{seg}_{YY}$	Area inertia moment of the segment about axes parallel to X and Y [m⁴]
$I^{sec}_{XX}; I^{sec}_{YY}$	Area inertia moment of the cross-section about the X and Y axes [m⁴]

$J; J^B_{eq}$	Effective shear stiffness [N]
K_s	Polar inertia moment; equivalent blade polar inertia moment [m⁴]
L, L_i	Length of WTB; length of the parts (i = 1, 2, 3, …) [m]
M	Mass of WTB [kg]
$q; q_o; q_{op}$	Shear flow; shear flow compatibility; open-section shear flow [N/m]
r	Relative contribution of shear deformation
s	Midline of the laminated shell
T	Torsional moment [N.m]
$\epsilon, \epsilon^{ply}_k$	Shell thickness; Thickness of laminate ply (k = 1, 2, 3, …) [m]
U	Shear strain energy [N.m]
$w(x, t)$	Transverse displacement [m]
X, Y	Elastic center of the cross-section
$x, y; \bar{x}, \bar{y}$	Coordinates of the segment; centroid of the segment
α	Ply orientation angle relative to the local axis (°)
β_n	Modal parameter for vibration mode (n = 1, 2, 3, 4) [1/m]
$\phi; \phi_{eq}$	Angle of twist of the variable-section WTB; angle of twist of the equivalent uniform beam [rad]
$\rho; \rho_{Seg}; \rho^{ply}_k$	Density; density of the segment; Density of the k-th composite ply [kg/m³]
$\kappa; \kappa^B_{eq}$	Shear correction factor; equivalent WTB Shear correction factor
$\kappa^{sec}_X; \kappa^{sec}_Y$	Shear correction factor of the section in X and Y direction
υ_{12}	Poisson's ratio of the laminate ply in the 1–2 directions

References

[1] Asef, M.R., Farrokhrouz, M., A Semi-Empirical Relation between Static and Dynamic Elastic Modulus, *Journal of Petroleum Science and Engineering*, 157, 2017, 359–363.
[2] Sahu, S.K., Das, P., Experimental and Numerical Studies on Vibration of Laminated Composite Beam with Transverse Multiple Cracks, *Mechanical Systems and Signal Processing*, 135, 2020, 106398.
[3] Ghoneam, S.M., Dynamic Analysis of Open Cracked Laminated Composite Beams, *Composite Structures*, 32, 1995, 3–11.

[4] Giaccu, G.F., Meloni, D., Concu, G., Valdes, M., Fragiacomo, M., Use of the Cantilever Beam Vibration Method for Determining the Elastic Properties of Maritime Pine Cross-Laminated Panels, *Engineering Structures*, 200, 2019, 109623.
[5] Guan, C., Zhang, H., Hunt, J.F., Yan, H., Determining Shear Modulus of Thin Wood Composite Materials Using a Cantilever Beam Vibration Method, *Construction and Building Materials*, 121, 2016, 285–289.
[6] Apsan, M.R., Mitu, A.M., Neagoe, C.A., Pop, N., Sireteanu, T., Non-Destructive Testing for Evaluation of Young's Modulus by Using Free Vibration Response of Composite Materials, *Applied Sciences*, 15, 2025, 10189.
[7] Loh, T.B., Wu, Y., Goh, S.H., Kong, K.H., Goh, K.L., Chong, J.J., An Integrated Approach for the Determination of Young's Modulus of a Cantilever Beam Using Finite Element Analysis and the Digital Image Correlation Technique, *Electronics*, 11, 2022, 2826.
[8] López-Puerto, A., Avilés, F., Gamboa, F., Oliva, A.I., A Vibrational Approach to Determine the Elastic Modulus of Individual Thin Films in Multilayers, *Thin Solid Films*, 565, 2014, 228–236.
[9] Lopez-Lopez, A., Robles-Ocampo, J.B., Lastres-Danguillecourt, O., Ibañez, G., Hernandez-Estrada, E., Sevilla-Camacho, P.Y., Novel Method for Determination the Dynamic Elastic Modulus of Composite Wind Turbine Blades, *Engineering Structures*, 312, 2024, 118254.
[10] Gruttmann, F., Wagner, W., Shear Correction Factors in Timoshenko's Beam Theory for Arbitrary Shaped Cross-Sections, *Computational Mechanics*, 27, 2001, 199–207.
[11] Ding, Y.Y., Bai, L.H., Chen, W.F., Liu, Y.P., Chan, S.L., A Generalized Method for Shear Correction Factors of Arbitrary Thin-Walled Sections, *Advanced Steel Construction*, 19, 2023, 223–241.
[12] Freund, J., Karakoç, A., Shear and Torsion Correction Factors of Timoshenko Beam Model for Generic Cross Sections, *Research on Engineering Structures and Materials*, 2, 2016, 19–27.
[13] Dong, S.B., Alpdogan, C., Taciroglu, E., Much Ado about Shear Correction Factors in Timoshenko Beam Theory, *International Journal of Solids and Structures*, 47, 2010, 1651–1665.
[14] Kirad, A., Zebbiche, T., Boun-Jad, M., Numerical Computation of Shear Stress in a Complex Cross Section Subjected to a Shear Force and Application to Airfoils, *Mechanics and Industry*, 17, 2016, 511.
[15] Zefouni, O., Kirad, A.E.K., Determination of the Shear Correction Factors of Complex Plane Sections for the Bending of Beams and Application to Airfoils, *Indian Journal of Physics*, 96, 2022, 2457–2466.
[16] D'Ottavio, M., Polit, O., *Classical, First Order, and Advanced Theories, Stability and Vibrations of Thin Walled Composite Structures*, Woodhead Publishing, 2017, 91–140.
[17] Hutchinson, J.R., Shear Coefficients for Timoshenko Beam Theory, *Journal of Applied Mechanics*, 68, 2001, 87–92.
[18] Banerjee, J.R., Kennedy, D., Elishakoff, I., Further Insights into the Timoshenko–Ehrenfest Beam Theory, *Journal of Vibration and Acoustics*, 144, 2022, 041014.
[19] Lopez-Lopez, A., Sánchez-Albores, R.M., Sevilla-Camacho, P.Y., Torres-Ventura, H.H., Rodríguez-Resendíz, J., Robles-Ocampo, J.B., Nonlinear Dynamic Analysis of Composite Wind Turbine Blades Using Lamination and Equivalent Beam Theory, *Journal of Applied and Computational Mechanics*, 2026, DOI: 10.22055/jacm.2026.48947.5616.
[20] Wang, L., Liu, X., Guo, L., Renevier, N., Stables, M., A Mathematical Model for Calculating Cross-Sectional Properties of Modern Wind Turbine Composite Blades, *Renewable Energy*, 64, 2014, 52–60.
[21] Zheng, T., Ji, T., Equivalent Representations of Beams with Periodically Variable Cross-Sections, *Engineering Structures*, 33, 2011, 706–719.
[22] Mahmoud, M.A., Dynamic Spring Constants of Higher Resonance Modes of Uniform and Tapered Microcantilevers with Tip Masses, *Micron*, 129, 2020, 102795.

ORCID iD

Andres Lopez-Lopez https://orcid.org/0000-0001-5707-9395
Jesus A. Enriquez-Santiago https://orcid.org/0000-0003-1318-6089
Marco A. Zuñiga-Reyes https://orcid.org/0000-0003-1549-232X
Marco A. Zamora-Antuñano https://orcid.org/ 0000-0002-9865-3944
Perla Y. Sevilla-Camacho https://orcid.org/0000-0002-9702-1929
José B. Robles-Ocampo https://orcid.org/0000-0002-0094-8710

How to cite this article: Lopez-Lopez A., et al. Experimental–Analytical Identification of Shear Elastic Modulus and Shear Correction Factor in Composite Wind Turbine Blades, *J. Appl. Comput. Mech.*, xx(x), 2026, 1–11. https://doi.org/10.22055/jacm.2026.49420.5964